Geol. Mag. **155** (*4*), *2018, pp. 797–810.* © *Cambridge University Press 2016*
doi:10.1017/S0016756816000996

Late Permian to Triassic isotope composition of sulfates in the Eastern Alps: palaeogeographic implications

ANA-VOICA BOJAR*‡†, STANISLAW HAŁAS§, HANS-PETER BOJAR‡ & ANDRZEJ TREMBACZOWSKI§

*Department of Geography and Geology, Salzburg University, Hellbrunnerstrasse 34, 5020 Salzburg, Austria
‡Department of Geoscience, Studienzentrum Naturkunde, Universalmuseum Joanneum, Weinzöttlstraße 16, 8045, Graz, Austria
§Mass Spectrometry Laboratory, Institute of Physics, Maria Curie-Skłodowska University, 20–031 Lublin, Poland

(*Received* 6 April 2016; *accepted* 28 September 2016; *first published online* 1 December 2016)

Abstract – Late Permian to Triassic phases from the evaporite deposits of the Northern Calcareous Alps (NCA) and Central Alpine Mesozoic (CAM) were analysed for sulfur and oxygen isotope compositions. For the Upper Permian, most of the $\delta^{34}S$ values are in the 11 to 12 ‰ range. Röt-type sulfates of Early Triassic age are characterized by a heavy sulfur isotopic composition of *c*. 26 ‰. The spatial compilation of the available data concerning the isotopic composition of Röt-type sulfates demonstrates that these evaporites are distributed over the entire area of the NCA. Their occurrences are associated with Early Triassic high-temperature conditions of the seawater and a widespread anoxia. The development of sulfates of Carnian–Norian age situated in the CAM is more modest; sulfates are characterized by a $\delta^{34}S$ value of *c*. 15 ‰. The $\delta^{18}O$ values show a broader distribution from 9 to 22 ‰, related to several factors such as type of deposit, recrystallization processes and bacterial sulfate reduction. The sulfate–sulfide thermometer applied to samples from NCA deposits indicates a thermal overprint of between 215 and 315 °C. Microbeam measurements support zonation of minor elements in sphalerite. Sphalerite microstructure indicates thermal overprinting, with no microbial structure being preserved.

Keywords: evaporites–sulfates, Röt type, sulfides, isotopic composition, thermal overprint, Permian–Triassic, Eastern Alps

1. Introduction

During Phanerozoic times, the concentrations of the main ions present in ocean water as Cl^-, SO_4^{2-}, HCO_3^-, Na^+, K^+, Mg^{2+} and Ca^{2+} have varied significantly. The variation of the ion concentration has been investigated over decades and has been the subject of continuous debates (Hardie, 1996; Kovalevich, Peryt & Petrichenko, 1998; Lowenstein *et al.* 2003; Holland, 2005; Lowenstein *et al.*, 2014; Algeo *et al.* 2015). For example, Permian seawater had a SO_4^{2-} concentration similar to that of modern seawater. Sulfate-rich marine waters were generally an exception in the history of the Earth and are restricted to late Precambrian (Vendian), Pennsylvanian–Triassic and Miocene to Quaternary times (Hardie, 1996). During such periods, potash deposits formed, which are characterized by the presence of $MgSO_4$ salts, such as polyhalite and kieserite. These periods have alternated with periods characterized by the formation of KCl salts, such as sylvite (KCl), as found in the Cambrian through Mississippian, and Jurassic through Palaeogene.

Sulfate minerals contain besides elements such as calcium, strontium, barium, magnesium and potassium also sulfur, oxygen and, in variable amounts, water. Sulfate evaporitic deposits represent important archives of Earth history, their formation indicating particular basinal and climatic conditions. Sulfur and oxygen stable isotope compositions of evaporites are controlled by global cycles through geological times as well as by local environmental factors. Thus, isotopic investigations on sulfur and oxygen from sulfate accumulations combined with mineralogical investigations may offer information regarding the origin of fluids, inflows or restricted conditions, evaporative effects, recrystallization and bacterial processes (Longinelli & Craig, 1967; Holser *et al.* 1979; Ohmoto, 1986; Hałas, 1987; Raab & Spiro, 1991; Machel, Krouse & Sassen, 1995; Seal, Alpers & Rye, 2000; Canfield, 2001; Kucha *et al.* 2010; Peryt, Hałas & Hryniv, 2010; Boschetti *et al.* 2011; García-Veigas *et al.* 2011).

The sulfur and oxygen isotopic composition of sulfate accumulations has varied in time and space. For example sulfur-isotope age curves for marine sulfate include the work of Nielsen (1965), Holser (1977), Claypool *et al.* (1980) and Strauss (1997). Sulfur-isotope age curves for structurally substituted sulfate in marine carbonate were also determined (Kampschulte & Strauss, 2004; Prokoph, Shields & Veizer, 2008), as well as a higher resolution record for Cretaceous barite accumulations (Paytan *et al.* 2004).

As the present study refers to evaporites of Late Permian – Triassic age, the general trends for this period of time will be summarized. The $\delta^{34}S$ values of sulfates

†Author for correspondence: ana-voica.bojar@sbg.ac.at

decreased towards the Late Permian (Nielsen, 1965; Holser, 1977; Claypool *et al.* 1980); a similar trend was also encountered for the $\delta^{18}O$ values of sulfates (Claypool *et al.* 1980). The isotopic composition of sulfur from oceanic sulfate is mainly controlled by a balance of the erosion input, mainly shales, as well as bacterial reduction and formation of sulfides. The low $\delta^{34}S$ values of Upper Permian sulfates are associated with the predominance of sulfur in oxidized phases, as gypsum or polyhalite. During the same time, carbon burial and the oxygen content of the atmosphere were high. Low isotopic values characteristic for marine sulfate of Late Permian age increased sharply during the formation of the Triassic Röt evaporites (Nielsen, 1965; Holser, 1977; Claypool *et al*. 1980). Besides general trends, significant isotopic variations of evaporitic sulfate as high as 3 ‰ were observed in different places within a given lithostratigraphic unit both vertically and horizontally, depending on a variety of depositional factors such as different degrees of restriction of the evaporitic basin to the open ocean, bacterial sulfate reduction in local evaporating basins and variation in terrigenic input (Claypool *et al.* 1980; Cortecci *et al.* 1981; Fanlo & Ayora, 1998; Longinelli & Flora, 2007). Post-depositional isotopic variations may be caused by the exchange of sulfate with water under higher temperature conditions that should affect the oxygen isotopes only. If thermal overprinting occurs in a practically closed system with a low water–rock ratio, the isotopic effects should be small for sulfur. Therefore, sulfur isotope composition is largely preserved during thermal overprinting, unless external fluids are involved.

Sulfur isotope compositions were earlier analysed for sulfates from the Permian–Triassic deposits of the Northern Calcareous Alps (NCA) (Pak, 1974, 1981; Spötl & Pak, 1996). As sulfate oxygen data have been missing up to now, the aims of the present study are to produce a new dataset of integrated sulfur and oxygen data for Permian–Triassic deposits situated in different units of the Eastern Alps. The data will provide information regarding the conditions of formation, regional extent and the subsequent history of the sulfate deposits.

2. Geology of investigated sulfate deposits

The Eastern Alps are characterized by the presence of three main tectonic units, the Lower, Middle and Upper Austroalpine, which overlie the Penninicum (Tollmann, 1977). The Upper Austroalpine unit consists of the NCA overlying the Greywacke zone and corresponding to the Graz Palaeozoic, Murau Palaeozoic and Gurktal nappe, with evaporitic rocks lacking in the later ones. The Mesozoic NCA belt is detached and thrust along the evaporitic Upper Permian to Lower Triassic Haselgebirge Formation. The sedimentation started in Late Carboniferous or Early Permian times, the youngest sediments being of Eocene age. The NCA are divided into the Bajuvaric, Tirolic and Juvavic nappe complexes. The evaporitic Haselgebirge Formation occurs in connection with the Juvavic nappe complex. Some evaporites are also situated in the Tirolic units (Leitner & Neubauer, 2011). The Haselgebirge Formation consists mainly of rock-salt, shales, gypsum and anhydrite and includes the oldest sediments of the NCA. The age of the Haselgebirge Formation, established by using spores and geochronological data, is Permian to Early Triassic (Klaus, 1965; Tollmann, 1977; Pak, 1974, 1981; Pak & Schauberger, 1981; Flügel & Neubauer, 1984; Schauberger, 1986; Spötl, 1988*a*; Spötl, 1989*a*; Weber, 1997; Schorn *et al.* 2013; Leitner *et al.* 2013). Palaeomagnetic investigations of Triassic to Lower Cretaceous deposits from the NCA indicate remagnetization during nappe stacking and folding events related to Alpine orogenesis (Pueyo *et al.* 2007).

In this study we investigated sulfates from halite and gypsum deposits; the regional distribution of samples is given in Figure 1. The deposits from where samples were taken are briefly presented below; the number corresponding to Figure 1 is indicated in brackets.

2.a. Salt deposits of the Northern Calcareous Alps sampled for this study

Hall in Tirol (1) is the westernmost salt-mine in the Eastern Alps and was closed in the 1960s after ~700 years of mining. It has an E–W extension of ~1 km. The deposit is situated at the base of the Tirolic unit next to the underlying Bajuvaric unit. The hosting rock, the so-called Haselgebirge, is a tectonic breccia of shales, sulfate rocks, rock-salt and sandstones. Sulfur isotope and palynological studies show a Late Permian age (Klaus, 1965). A second evaporitic event occurred during Anisian time and is represented by dolomite/anhydrite rocks (Pak, 1974; Spötl, 1988*a*,*b*; Spötl, 1989*b*; Weber, 1997; Leitner & Neubauer, 2011).

The *Hallein/Dürnberg* (2) deposit is interconnected with the salt deposit in Berchtesgaden, Germany. The ore body extends from SW–NE with a length of ~ 7 km and is up to 2 km wide. The base of the salt body is ~ 1 km deep below the surface. The deposit is situated between a lower Tirolic and an upper Juvavic nappe and has a Late Permian age (Gawlick *et al*. 1999). The salt incorporated Lower Triassic to Jurassic host rocks (Leitner & Neubauer, 2011).

The *Hallstatt* (3) and Dürrnberg deposits have been mined since the Bronze Age. The Hallstatt deposit is also well known as it is named after the Hallstatt culture stage. The deposit extends E–W and is 3 km in length and 600 m in width. Host-rock incorporations include besides Permian volcanic rocks also Triassic to Jurassic rocks (Gawlick *et al*. 2001; Leitner & Neubauer, 2011).

Altaussee (4) is an actively mined rock-salt deposit which covers an area of ~ 2.3 km^2. A *c*. 1 km deep drilling did not reach the bottom of the deposit. The

https://doi.org/10.1017/S0016756816000996 Published online by Cambridge University Press

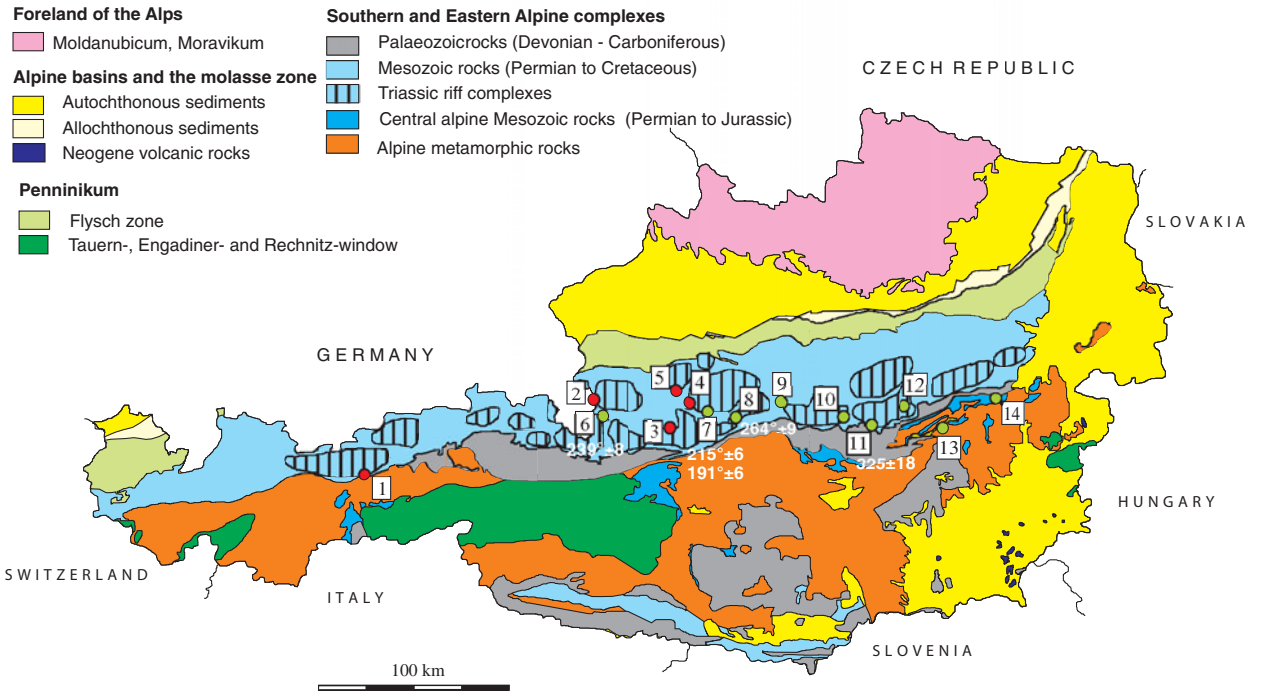

Figure 1. (Colour online) Geological overview of the Eastern Alps showing the distribution of investigated sulfate accumulations. Distribution of calculated temperatures using sulfur isotope composition (Table 4). Salt: 1 – Hall in Tirol; 2 – Hallein; 3 – Hallstatt; 4 – Altaussee; 5 – Bad Ischl. Gypsum deposits, Northern Calcareous Alps: 6 – Golling; 7 – Wienern; 8 – Lessern; 9 – Unterlaussa; 10 – Wildalpen; 11 – Tragöß; 12 – Seewiesen. Gypsum deposits, Central Alpine Mesozoic: 13 – Stanz; 14 – Göstritz.

only host rocks incorporated in the rock-salt are of the Triassic Hallstatt formation (Leitner & Neubauer, 2011). The deposit is covered by the Middle Jurassic Sandling-Alm Formation (Gawlick, Schlagintweit & Suzuki, 2007).

Bad Ischl is a rather small (~ 0.5 km^2) rock-salt deposit. The deposit is jammed between Triassic, Jurassic and Cretaceous rocks. Rocks incorporated to the rock-salt are Permian volcanic rocks, Triassic rocks from the Hallstatt formation and Cretaceous sandstones and conglomerates (Leitner & Neubauer, 2011).

2.b. Gypsum deposits of the Northern Calcareous Alps sampled for this study

Numerous, partly mined sulfate deposits occur along with the rock-salt deposits of the NCA. Besides the major phases of gypsum and anhydrite, a large number of sulfide phases like galenite, sphalerite, pyrite, lead-arsen-sulfosalts, tennantite and native sulfur a.s.o. are reported frequently. Carbonates such as magnesite, dolomite and calcite can be found either as singular crystals (Kirchner, 1987; Niedermayr, Beran & Brandstätter, 1989) or as small accumulations within the hosting gypsum. Gabbroic intrusive and volcanic rocks are common in the western gypsum deposits of the NCA.

The *Golling/Moosegg* deposit is located in the Juvavic unit of the NCA. The deposit has a poorly constrained age of Late Permian, using stable sulfur isotope data (Pak, 1978). The main Haselgebirge body comprises foliated, massive and brecciated anhydrite and gypsum. For the Late Permian period, rifting with a half-graben structure is proposed. In an advanced stage of the rifting gabbroic rocks intruded into a high crustal level; even a few volcanic rocks are known. The volcanic rocks are in close contact with the Haselgebirge; therefore, they are interpreted as syngenetic (Schorn & Neubauer, 2011; Schorn *et al.* 2012)

The *Wienern/Grundlsee* gypsum deposit is situated at the base of the Hallstätter nappe, which is part of the Juvavicum. Some tens of metres of gypsum encase an anhydrite body. A pumpellyite-bearing pillow-lava breccia has been observed at the base of the deposit (Haditsch, 1968; Kirchner, 1979).

Lessern and *Wildalpen* are small gypsum accumulations within the Werfener strata. Geological descriptions are scarce. More than 50 gypsum occurrences are observed only in the eastern part of the NCA (Weber, 1997). A gypsum occurrence some kilometres east of Lessern (close to Stainach, Styria) was classified with spores as Late Permian (Klaus & Pak, 1974).

Tragöß/Haringgraben: The Upper Permian Haselgebirge Formation at Haringgraben represents a *c.* 100 m thick wedge and hosts one of the largest gypsum/anhydrite deposits of the Eastern Alps. It is stratigraphically situated above the younger, Scythian, Werferner Slates. These units are overlain by a thick carbonate sequence (Wetterstein Formation of Triassic age) (Kölbl & Gawlick, 1999). Sulfides (sphalerite, galenite, pyrite), sulfarsenides (enargite, baumhauerite) and native sulfur enrichments are known (Postl, 1990).

https://doi.org/10.1017/S0016756816000996 Published online by Cambridge University Press

2.c. Gypsum deposits of the Central Alpine Mesozoic sampled for this study

The Central Alpine Mesozoic (CAM) hosts a second evaporative zone. Geographically it is situated along with the mostly amphibolite-facies metamorphic crystalline of the Lower Austroalpine nappes from the Semmering area.

Stanz: The gypsum deposit of the Stanz valley is one of the Central Alpine deposits sampled for this study and it lies within a Lower to Upper Triassic unit. The Triassic of the Stanz valley is a few hundreds of metres wide stripe with Scythian quartzites, Anisian rauhwacke and Anisian and Ladinian Muschelkalk. Host rocks of the Triassic series are gneisses, micaschists and quartz-phyllites of the Lower and Middle Austroalpine nappes. The deposit consists of a tens of metres wide anhydrite core, encased by gypsum. The gypsum body is most probably of Carnian or Norian age (Bauer, 1967; Hagenguth, 1988).

Göstritztal/Schottwien: Two Central Alpine gypsum deposits are found in the Semmering area: Haidbachgraben and Göstritz. The samples investigated in this study are from the Göstritz valley. Characteristic rocks of the Semmering–Triassic are violet and green Keuper sericite schists with gypsum intercalations. Age data like classification with spores are lacking, but a Carnian age is the most probable. Similar to the Stanz valley deposit, an anhydrite core is enclosed by a gypsum rim. The immediate wall rocks of the Göstritz deposit are Rhaetian dolomites, violet sericite schists, Keuper quartzite and Rhaetian black-shales and limestones (Bauer, 1967).

3. Material and methods

Descriptions of the analysed material, mineral associations, as well as data on stratigraphic age and location are given in the online Supplementary Material available at http://journals.cambridge.org/geo and Tables 1 and 2. Isotopic data on sulfates, sulfides and carbonates are displayed in Table 1. In Table 3 calculated temperatures using sulfur isotope distributions in sulfate, sulfides and sulfur are given.

The isotope ratios of sulfates ($\delta^{34}S$ and $\delta^{18}O$) and sulfides ($\delta^{34}S$) were determined by measuring the isotopic composition of resulting SO_2 and CO_2 gases on a dual-inlet and triple collector mass spectrometer. Sulfur in the form of SO_2 gas was quantitatively extracted from $BaSO_4$ samples by thermal decomposition at 850 °C in a Cu boat in the presence of Na_2PO_4 reagent (Hałas & Szaran, 2001, 2004). CO_2 gas was prepared by graphite reduction with conversion of CO to CO_2 by glow discharge (Mizutani, 1971). Nearly quantitative CO to CO_2 conversion was attained using a magnetic field in the conversion unit (Hałas *et al.* 2007). Rough delta values were normalized to the VCDT and the VSMOW scales by analysis of the SO_2 and CO_2 raw isotopic ratios prepared from the NBS-127 standard, for which we assumed $\delta^{34}S$ = 21.17 ‰ (Hałas & Szaran, 2001) and $\delta^{18}O$ = 8.73 ‰ (Hałas *et al.* 2007).

For carbonate samples, the $\delta^{13}C$ and $\delta^{18}O$ values were determined as well. CO_2 gas was extracted from calcite at 25 °C by reaction with H_3PO_4 (McCrea, 1950) and measured on an isotope-ratio mass spectrometer with dual-inlet system. Standard deviations of measurements for the NBS19 international standard were better than 0.1 ‰. Delta values were normalized to the Vienna Pee-Dee Belemnite (VPDB). For a rigorous discussion regarding the relationship between SMOW and VSMOW see Sharp (2014).

Polished sections of sphalerite where analysed with a Jeol 6610 LV scanning electron microscope equipped with an Oxford WDS 700 spectrometer (20 keV, beam current 20 μA, standards Zn, S: sphalerite, Fe: pyrite, Mn: metallic manganese, Cd: metallic cadmium). The results given in Table 4 are a median of ten analyses each.

4. Results

4.a. Stable isotope data

The total number of investigated phases is 54, including analyses on sulfates, sulfides, sulfur and carbonates. The locations of the samples are shown in Figure 1. A total of 34 sulfates were investigated, and oxygen and sulfur isotopic composition were determined for anhydrite, gypsum, polyhalite and langbeinite. The samples containing the investigated phases are described in the online Supplementary Material available at http://journals.cambridge.org/geo and data are given in Table 1. The $\delta^{34}S$ values vary between 10.1 and 16 ‰ (VCDT), with two higher values of 20.5 and 26.6 ‰. The $\delta^{18}O$ values range from 9 to 23 ‰ (VSMOW) (Figs 2, 3a, b). The $\delta^{34}S$ values of 14 sulfides (galenite, sphalerite, pyrite) as well as native sulfur range between −17.5 and 2.8 ‰ (VCDT). The $\delta^{13}C$ and $\delta^{18}O$ values were determined for five carbonates as well.

In Figure 2 the isotopic composition of sulfur and oxygen is plotted, differentiated for the different locations of the samples. For comparison, the field covering the present-day isotopic composition for marine sulfates is given as well. The investigated Upper Permian to Triassic sulfates may be divided in three groups with different mean $\delta^{34}S$ and $\delta^{18}O$ values as follow: (a) from the Permian halite-type deposits of the NCA with mean $\delta^{34}S$ and $\delta^{18}O$ values of 11.8 ‰ and 16.6 ‰, respectively; (b) from the Permian gypsum deposits of the NCA with mean $\delta^{34}S$ and $\delta^{18}O$ values of 12.6 ‰ and 14.5 ‰, respectively; (c) from the Triassic CAM with mean $\delta^{34}S$ and $\delta^{18}O$ values of 14.8 ‰ and 16.5 ‰, respectively.

4.b. Microbeam measurement of sphalerite

In the online Supplementary Material available at http://journals.cambridge.org/geo the measured

https://doi.org/10.1017/S0016756816000996 Published online by Cambridge University Press

Table 1. Isotopic composition of sulfate and sulfides from the investigated evaporitic deposits

Locality	Age	Sample	Mineral	δ^{34}S ‰ (VCDT)	δ^{18}O ‰ (VSMOW) sulfate	δ^{18}O ‰ (VSMOW) carbonate	δ^{13} C‰ (VPDB)
Salt, NCA							
Hall in Tirol	Late Permian and Anisian	HT_1	anhydrite	11.0	22.7		
		HT_2	gypsum	10.2	13.1		
Hallein (Dürrenberg)	Late Permian	D_1	polyhalite	20.4	19.6		
		D_2	polyhalite	11.6	17.8		
		D_3	anhydrite	13.2	21.7		
Hallstatt	Late Permian	H_1	polyhalite	10.3	16.0		
		H_2	blödite	12.5	17.8		
		H_4	gypsum	10.4	14.5		
Altausee	Late Permian	A_1	polyhalite	11.5	18.8		
		A_2	anhydrite	10.5	13.8		
		A_3	anhydrite	11.5	12.5		
		A_4	gypsum	12.4	16.1		
		A_5	gypsum	12.7	17.1		
Bad Ischl	Late Permian	BI_1	polyhalite, vein	14.6	18.4		
		BI_2	polyhalite	12.1	12.5		
Gypsum, NCA							
Golling		G_2	gypsum	16.0	15.8		
		G_1	sulfur	−10			
		G_3	dolomite			23.6	−7.4
		G_4	gypsum	11.67	19.8		
Wienern		W_2	dolomite			21.7	−3.5
		W_3	gypsum	13.9	8.4		
		W_4	pyrite	2.8			
		W_5	magnesite			33.6	−8.1
		W_6	galenite	−17.5			
		W_7	sphalerite	−16.7			
		W_8	gypsum	13.3	13.1		
		W_9	gypsum	11.06	14.7		
Lessern	Late Permian	L_2	gypsum	15	16.5		
		L_1	sulfur	−9			
Unterlaussa		Wd_3	gypsum	26.4	14.6		
Wildalpen		Wd_1	gypsum	11.3	14.9		
Tragöß	Late Permian	T_1	galena	−13.4			
		T_2	sphalerite	−12.5			
		T_3	pyrite	−9.9			
		T_4	sulfur	−14.8			
		T_5	gypsum	11.2	20.0		
		T_6	anhydrite	10.9	13.6		
		T_7	Gypsum	11.6	12.8		
		T_8	dolomite			23	2.6
		T_8/1	sphalerite	−9.6			
		T_8	gypsum	14.0	11.5		
		T_9	dolomite			23.0	3.2
		T_10	sphalerite	−5.4			
		T_11	gypsum	13.2	12.6		
		T_12	sphalerite	−7.5			
		T_13	sphalerite	−7.8			
		T_14	dolomite			26.9	4.5
		T_15	pyrite	−4.8			
Seewiesen		Wd_2	gypsum	11.3	14.3		
Gypsum, CAM							
Stanz	Triassic (Carnian-Norian)	St_1	anhydrite	14.4	15.6		
		St_2	gypsum	14.2	14.7		
Göstritz	Triassic (Carnian)	Gt_1	anhydrite	14.8	15.8		
		Gt_2	gypsum	15.5	15.6		
		Gt_3	dolomite				
		Gt_4	gypsum	15.1	20.8		

sphalerite crystal is outlined by a red square. This crystal shows a strong zonation in colour: a brownish core, a yellowish intermediate section and a reddish rim. The results are given in Table 4, representing an average of ten analyses each. The minor component concentrations are low. Cadmium has an average concentration of ∼ 0.50 wt %/∼ 0.20 at. % irrespective of the position. In contrast manganese and iron show a strong zonation. Iron is concentrated in the core. The average content is 2.35 wt %/1.99 at. %. However, the iron

https://doi.org/10.1017/S0016756816000996 Published online by Cambridge University Press

Table 2. Localities of the NCA with 'Röt-type' $\delta^{34}S$ values

Locality	$\delta^{34}S$ (VCDT)	
Hall in Tirol	24.6, 24.6, 25.6, 25, 27.1, 24.5, 23.9, 24.7	Spötl, 1988*c*
	25	Pak & Schauberger, 1981
Reichenhall	25.4	Pak, 1974; Pak & Schauberger, 1981
Bad Ischl	26.7	Pak & Schauberger, 1981
Teichelbachgraben W Bad Ischl	24.2	Pak & Schauberger, 1981
Hallstatt	27.4	Spötl & Pak, 1996
	26.8	Pak & Schauberger, 1981; Pak, 1981
Windischgarsten	26.2	Pak & Schauberger, 1981
Bosruck-Tunnel	28.1	Pak & Schauberger, 1981
Anzenauer Weißenbachtal	22.7	Pak & Schauberger, 1981
Lachwaldspitze beim Achensee	25.6	Pak, 1974; Pak & Schauberger, 1981
Sulzgraben SW Plumsjoch am Achensee	23.9	Pak & Schauberger, 1981
SE-Fuß des Kapuzinerberg, Salzburg Stadt	21.9	Pak & Schauberger, 1981
Trübenbach	23.5	Götzinger & Pak, 1983
Brandgegend	25.4	Seemann & Pak, unpub. (in Götzinger & Pak, 1983)
Dristl-Alm SW Pertisau	23.3, 24.2	Spötl, 1988*a*
Wienern	24.3	Spötl & Pak, 1996
Schildmauer	25.8, 26.7	Spötl & Pak, 1996
Kaswassergraben	27.2	Spötl & Pak, 1996
	25.4	Erkan, 1989
	27.6	Niedermayr, Beran & Brandstätter, 1989
Palbersdorf bei Aflenz	26.4	Pak, 1978
Unterlaussa	26.4	this study

Table 3. Calculated temperatures using sulfur isotope distributions in sulfate, sulfides and sulfur

Locality	Sample	Mineral	$\delta^{34}S$ (VCDT)	T °C using $\delta^{34}S$ of sulfate–sulfides
Golling	G_2	gypsum	16.0	gypsum–sulfur: 239 ± 8
	G_1	sulfur	− 10	(Ohmoto & Rye, 1979)
Wienern	W_6	galena	− 17.5	gypsum–galena: 215 ± 6
	W_7	sphalerite (III, red)	− 16.7	gypsum–sphalerite (III): 191 ± 6
	W_8	gypsum	13.3	(Ohmoto & Rye, 1979)
Lessern	L_2	gypsum	15	gypsum–sulfur: 264 ± 9
	L_1	sulfur	− 9	(Ohmoto & Rye, 1979)
Tragöß	T_1	galena	− 13.4	pyrite–galena: 270 ± 46 (Ohmoto & Rye, 1979); 283 ± 47 (Kajiwara & Krouse, 1971)
	T_2	sphalerite (III, red, rim)	− 12.5	pyrite–sphalerite (III): 165 ± 84 (Ohmoto & Rye, 1979); 67 ± 12 (Kajiwara & Krouse, 1971)
	T_3	pyrite	− 9.9	
	T_8/1	sphalerite (III, red, rim)	− 9.6	gypsum–sphalerite (III): 280 ± 10
	T_8	gypsum	14	(Ohmoto & Rye, 1979)
	T_10	sphalerite (II, yellow, grown on the dark sphalerite, between dark and red)	− 5.4	gypsum–pyrite: 363 ± 13 (Ohmoto & Rye, 1979)
	T_11	gypsum	13.2	gypsum–sphalerite (III): 313 ± 12 (Ohmoto & Rye, 1979) gypsum–sphalerite (I): 316 ± 12 (Ohmoto & Rye, 1979) gypsum–sphalerite (II): >400 (Ohmoto & Rye, 1979)
	T_12	sphalerite (I, core, dark)	− 7.5	pyrite–sphalerite (II): >400 (Ohmoto & Rye, 1979)
	T_13	sphalerite (III, rim, red)	− 7.8	pyrite–sphalerite (I): 183 ± 94 (Ohmoto & Rye, 1979)
	T_15	pyrite	− 4.8	pyrite–sphalerite (III): 157 ± 80 (Ohmoto & Rye, 1979)

content ranges from 0.4 to 5.88 wt %, with patches of high iron concentrations in a matrix with a lower iron concentration. The core also frequently has small inclusions of pyrite. The manganese concentration is low, close to the detection limit. In contrast the iron content of the outer reddish zone is below the detection limit and the manganese content is enriched compared to the core zone (0.50 wt %/0.36 at. % Mn). The narrow yellowish intermediate zone has low iron (0.10 wt %/0.05 at. %) and low manganese contents (0.06 wt %/0.05 at. %). Other monitored minor elements like (As, Se) were below the detection limit.

5. Discussion

The oxygen isotopic exchange rate is low between dissolved sulfate and water at temperatures below 200 °C (Chiba & Sakai, 1985; Seal, Alpers & Rye, 2000). The sulfur and oxygen isotopic composition of sulfates should reflect the composition of dissolved sulfates,

https://doi.org/10.1017/S0016756816000996 Published online by Cambridge University Press

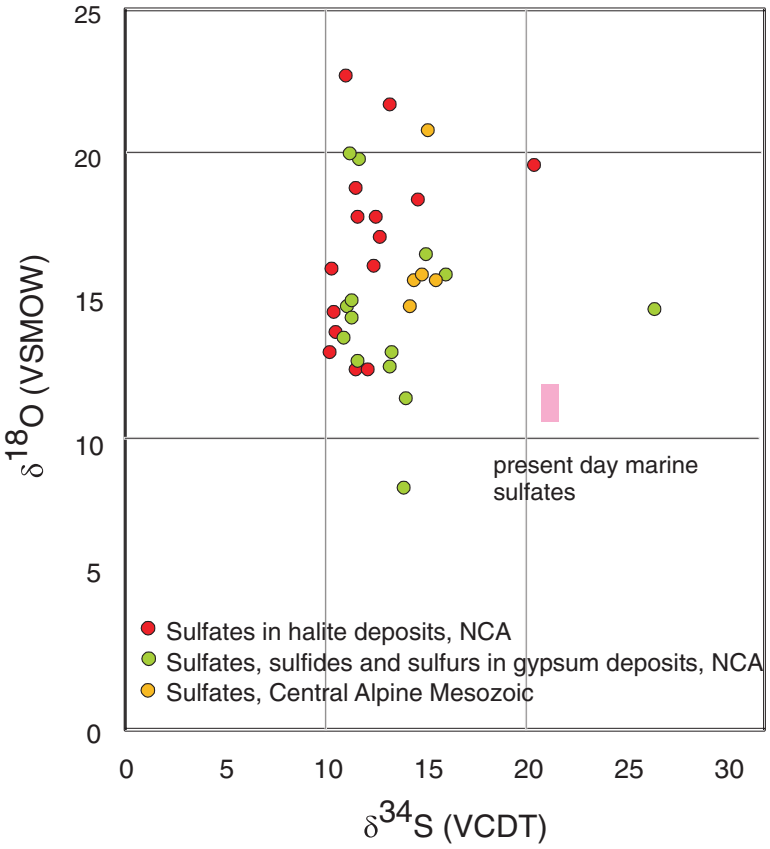

Figure 2. (Colour online) δ^{34}S and δ^{18}O values of measured sulfate. The red circles represent sulfates from the halite deposits; the green circles represent sulfates from gypsum deposits. The rectangle represents the isotope value of sulfate precipitated from marine water.

Table 4. Electron microbeam analyses of sphalerite zonation from sample T1, Tragöß

weight %	**core**	**interm.**	**rim**
Zn	62.87	66.14	65.66
Mn	0.02	0.06	0.41
Fe	2.35	0.10	b.d.l.
Cd	0.50	0.56	0.50
S	35.00	33.64	33.50
sum	100.74	100.50	100.07
atomic%			
Zn	45.84	48.90	48.74
Mn	0.01	0.05	0.36
Fe	1.99	0.09	-
Cd	0.21	0.24	0.22
S	51.95	50.72	50.68

b.d.l. – below the detection limit

and not the composition of water. Besides temperature, the exchange rate is also dependent on pH (Chiba & Sakai, 1985).

Dissolved sulfate in modern seawater has a δ^{34}S value of +21 ‰ (Rees, Junkins & Monster, 1978; Longinelli, 1983; Böttcher, Brumsack & Dürselen, 2007), but its composition has varied in ocean history related to bacterial reduction and continental weathering (Claypool *et al.* 1980). The δ^{34}S of the seawater sulfate is *c.* 1.7 ‰ less than that of the precipitated mineral (Thode & Monster, 1965). In a more detailed study, Szaran, Niezgoda & Hałas (1998) proposed a value of 1.54 ± 0.09 ‰. Therefore, sulfur fractionation between sulfate minerals and aqueous sulfates is small, as was underlined by several authors (Ault & Kulp, 1959; Holser & Kaplan, 1966; Sakai, 1968; Raab & Spiro, 1991). The δ^{18}O value of the present-day dissolved marine sulfate is *c.* 9.5 ‰ (Longinelli & Craig, 1967; Rafter & Mizutani, 1967; Longinelli, 1983), the value of precipitated sulfate being 3.5 ‰ heavier than the dissolved sulfate, thus *c.* 13 ‰ (Gonfiantini & Fontes, 1963; Lloyd, 1968) A more recent study by Szaran, Niezgoda & Hałas (1998) led to considering an even smaller fractionation value of 2.90 ± 0.09 ‰.

Upper Permian seawater sulfates are characterized by low δ^{34}S values between 10 and 13 ‰ (Claypool, 1980). For the Permian, sulfur isotopic composition of the sulfate group from calcitic brachiopod shells shows a higher mean of 13.2 ± 2.5 ‰ (Kampschulte & Strauss, 2004). In the present study, the distribution of δ^{34}S values of sulfates from both halite- and gypsum-type deposits of the NCA have values of 11.8 ‰ and 12.6 ‰, respectively, in the range determined by Claypool *et al.* (1980) for Late Permian time. For the NCA, there are a few values higher than 13 ‰, as for example D_1, BI_1, G_2, W_3 and L_2; in all the cases sulfates are associated with vein or vug filling, thus with remobilization. Interestingly, not all the remobilized sulfates (for example H_4 or A_5) are associated with higher values, instead they have values in the range of 10 to

https://doi.org/10.1017/S0016756816000996 Published online by Cambridge University Press

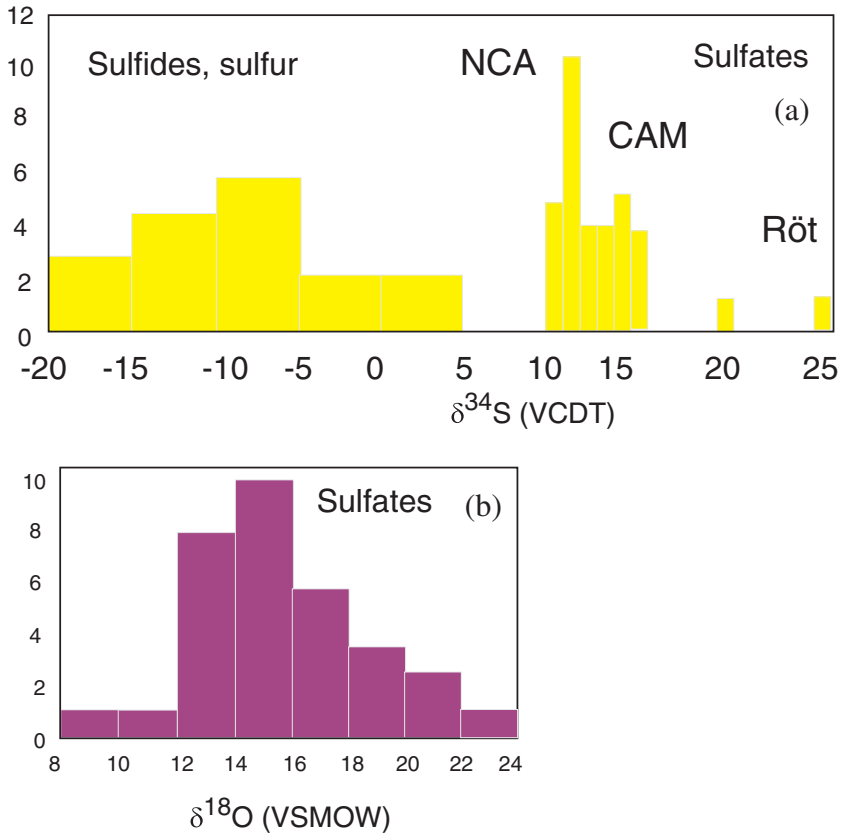

Figure 3. (Colour online) Histograms representing: (a) sulfur isotopic distribution of sulfate, sulfide and sulfur from evaporite deposits; (b) oxygen isotopic distribution of sulfate. All values are measured in this study.

13 ‰. The measured δ^{34}S values of sulfates for both types of deposits, halite and gypsum from the NCA, show a maxima between 11 and 12 ‰. For sulfates of the Haselgebirge, Spötl & Pak (1996) determined the maxima in the same range (Fig. 4 this study is plotted from table 1 in Spötl & Pak, 1996). Similar maxima, between 11 and 12 ‰, were determined for the Upper Permian anhydrite of western Poland (Peryt, Hałas & Hryniv, 2010), for Permian Zechstein anhydrites of northern Germany (Kampschulte, Buhl & Strauss, 1998) and for the Upper Permian metamorphosed anhydrites from Italy (Cortecci *et al.* 1981). A larger δ^{34}S range of about 8 ‰ was observed for Keuper sulfate in northern-central Europe, with δ^{34}S values decreasing on average from Germany to Denmark (Nielsen, 1989). The δ^{18}O values display a larger scatter from 9 to 23 ‰, which is even larger than that found for the Upper Permian anhydrites of northern Germany, the Italian Alps or western Poland (Cortecci *et al.* 1981; Kampschulte, Buhl & Strauss, 1998; Longinelli & Flora, 2007; Peryt, Hałas & Hryniv, 2010). The mean value for δ^{18}O of sulfate from the halite-type deposits is 16.6 ‰, higher than in the gypsum-type deposits, with a mean of 14.5 ‰. For the halite-type deposits, there is a correlation between the sulfur and oxygen isotope composition, with the equation of the best fit line $y = 1.25x + 1.34$, $R^2 = 0.34$. This may support that bacterial sulfate reduction affected both sulfur and oxygen isotopic composition of sulfates. Sulfate-reducing bacteria can substantially enhance the oxygen isotope exchange rate between sulfate and water (Fritz *et al.* 1989; Grinenko & Ustinov, 1991) and change the isotopic signature of precipitated sulfates. For the gypsum-type deposit no significant correlation between sulfur and oxygen isotopic values could be put in evidence. This suggests that (besides bacterial sulfate reduction) another mechanism was involved for the variable oxygen isotopic values, most likely the oxygen isotope exchange with brine water over the long residence time of the sulfate ions (Hałas & Pluta, 2000; Zeebe, 2010; Boschetti, 2013). With increasing temperature, isotopic equilibration of oxygen will lower fractionation between sulfate and water, which are in disequilibrium at ambient temperatures. In the present study, the lowest measured oxygen isotope values are *c.* 12 ‰, in the range of values indicated by Claypool *et al.* (1980) for the Upper Permian sulfates. Equilibration during thermal overprinting, for example during dehydration of gypsum to anhydrite, will lower the δ^{18}O value of sulfate, assuming a near marine isotopic composition of water. In the present case, as shown in Figure 2, the δ^{18}O values of sulfates show a trend from values of 12 ‰ towards higher values, up to 23 ‰. This pattern excludes isotopic re-equilibration at high temperature as an explanation for the observed shift. Instead, the shift towards

https://doi.org/10.1017/S0016756816000996 Published online by Cambridge University Press

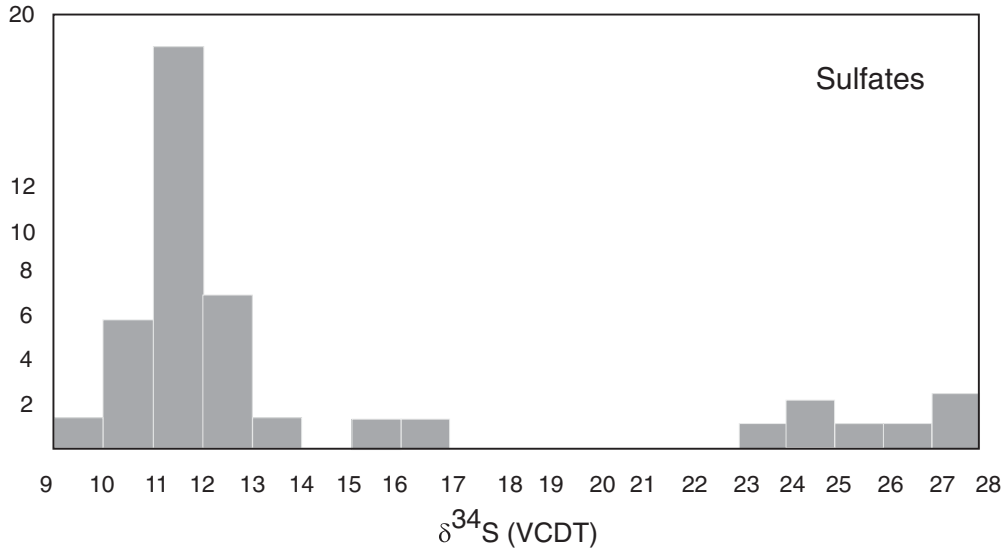

Figure 4. Histogram representing sulfur isotopic distribution for sulfates and sulfides, data after Spötl & Pak (1996, their table 1).

higher values may be related to recrystallization at relatively low temperatures (30–35 °C; Hałas & Pluta, 2000).

The associated carbonates, as calcite, dolomite and magnesite, are in isotopic disequilibrium with sulfates, the isotopic signature of the carbonates indicating rather a primary marine isotopic signature (Table 1) than re-equilibration with sulfates at higher temperatures.

Nielsen (1965) mentioned that the so-called Röt-type gypsum of Early Triassic age, measured in deposits of Germany and the Netherlands, have a strikingly high isotopic $^{34}S/^{32}S$ ratio in comparison to those from the Upper Permian. Nielsen (1965) associated such high values with the presence of local, closed basins characterized by high bacterial activity. The sharp increase of the $\delta^{34}S$ values from Late Permian to Early Triassic times is considered by Holser (1977) to be 'the result of … fast net sulfide deposition'. In the present study, a gypsum from Unterlausa (Table 1) shows a high $\delta^{34}S$ value of 26.4 ‰. Similar high values were measured by Pak (1974, 1978, 1981), Pak & Schauberger (1981), Götzinger & Pak (1983), Spötl (1988*a*, *c*), Erkan (1989), Niedermayr, Beran & Brandstätter (1989) and Spötl & Pak (1996) for evaporites situated in the NCA (Table 2). Our compilation of data for the Röt-type gypsum from the literature (Table 2; Fig. 5) supports the presence of Lower Triassic evaporites, over a larger area than previously estimated. The $\delta^{34}S$ values determined for the NCA are lower than those determined for Röt-type evaporites in the Netherlands, Germany and Poland, varying between 27 and 31 ‰ (Scholle *et al*. 1995). A characteristic feature of the Unterlausa gypsum is the fine-grained texture and the grey colour. X-ray diffraction (XRD) analyses indicate pure gypsum with no visible crystallized detrital components such as quartz or feldspar. According to Kovalevych *et al.* (2002) the Röt evaporites were deposited in the E–W-oriented German Basin, which extended from the UK offshore to western Poland. The data compilation displayed in Figure 5 clearly demonstrates the presence of this type of Lower Triassic evaporites also occurring in an E–W trend along the NCA. Recent investigations by Rey *et al.* (2016) have shown that land and ocean temperatures strongly fluctuated during Late Permian to Early Triassic times. Moreover, we can correlate the formation of Röt-type evaporites with a temperature maximum during Early Triassic time, as documented by Rey *et al.* (2016). From the point of view of ocean chemistry, during the deposition of the Röt evaporites, the concentration of the sulfate ions in seawater was intermediate between the high value, typical for Late Permian seas, and the low value typical for Late Triassic seas (Kovalevych *et al.* 2002). Worldwide at the level of the Lower Triassic, the perturbation of the carbon cycle and carbon positive excursion were evidenced by Payne *et al.* (2004). The carbon isotopic excursions reflecting major perturbations after the Permian–Triassic extinction event were correlated with ocean anoxia (Song *et al.* 2012). In the light of present investigations and available studies, we suggest that Röt-type evaporites were formed in a large intracontinental stratified sea, with limited connection to the ocean during oscillations following the Permian–Triassic mass extinction.

The Upper Triassic evaporites of Carnian–Norian ages from the CAM show a narrow range of $\delta^{34}S$ values, close to 15 ‰. Claypool *et al.* (1980) indicated values between 15 ‰ and 17 ‰ from the Middle Triassic to Jurassic. The oxygen isotope composition for the Lower Triassic Röt-type evaporites and for the Upper Triassic evaporites is similar: between 15 ‰ and 16 ‰. One exception is represented by the Gt_4 sample, from Göstritz (CAM), a joint fill gypsum, with a $\delta^{18}O$ value of 20.8 ‰ supporting oxygen isotopic exchange with brine water during recrystallization.

https://doi.org/10.1017/S0016756816000996 Published online by Cambridge University Press

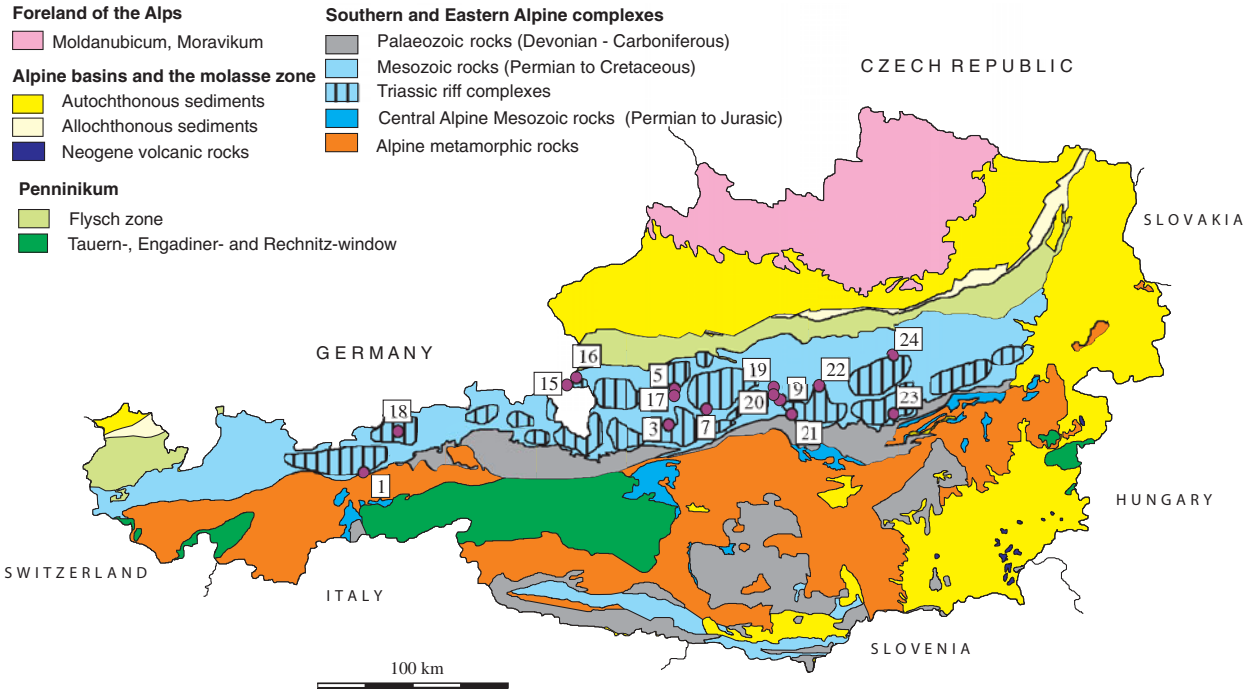

Figure 5. (Colour online) Distribution of Lower Triassic 'Röt-type' gypsum (see also Table 3): 1 – Hall in Tirol; 3 – Hallstatt; 5 – Bad Ischl, Teichelbachgraben; 7 – Wienern; 9 – Unterlaussa; 15 – Bad Reichenhall; 16 – Kapuzinerberg Salzburg; 17 – Anzenau Weißenbach; 18 – Pertisau Achensee; 19 – Windischgarsten; 20 – Bosruck-Tunnel; 21 – Schildmauer bei Admont; 22 – Palbersdorf bei Aflenz; 23 – Brandgegend, Trübenbach.

When present in visible amounts, sulfides were separated and concentrated. The broad distribution of sulfide $\delta^{34}S$ values points towards bacterial reduction of the sulfate group (Berner, 1985). During this process, various sulfides, depending on the available cations, were formed. The investigated evaporitic deposits from the NCA were overprinted during burial at higher temperatures (Leitner *et al.* 2013; Schorn *et al.* 2013). We used the sulfate–sulfide and sulfide–sulfide isotopic data in order to calculate the overprint temperatures. The calculated temperatures and associated errors are given in Table 3, for sulfate–sulfide and sulfide–sulfide mineral pairs. The sulfide–sulfide calculated temperatures have larger errors owing to the small isotopic fractionation between various sulfides. For Golling, Wienern and Lessern, the sulfate–sulfide thermometer shows a narrow range of thermal overprint between 215 and 264 °C. For Tragöß, the most reliable calculated temperatures, sulfate–sulfide, are higher, between 280 and 360 °C. The temperature calculated using the Ohmoto & Rye (1979) calibration and the sulfur isotopic composition of the yellowish sphalerite (II) is considered unrealistically high, reflecting isotopic disequilibrium. For the pyrite–galena mineral pair, the calculated temperatures are similar using either the Kajiwara & Krouse (1971) or Ohmoto & Rye (1979) calibrations (Table 3). For the pyrite–sphalerite mineral pair, temperatures are much higher using the Ohmoto & Rye (1979) and lower using the Kajiwara & Krouse (1971) calibrations (Table 3). A recent calibration is available for the system pyrite–H_2S (Syverson *et al.* 2015). In this new calibration, the 'a' factor of the temperature equation is −0.737 instead +0.4 as given previously in the equation determined by Ohmoto & Rye (1979). No similar recent calibrations are available for other sulfides as sphalerite or galena, so for the moment, the data of Syverson *et al.* (2015) could be not applied in calculating mineral pair temperatures. If changes of a similar magnitude and sign for the 'a' factor from the temperature equation are expected for the other sulfides, then the calculated temperatures using the mineral pairs will not differ significantly.

Microbeam measurements show a zonation of minor elements in sphalerite (Tragöß, sample T_1, Tables 1, 4). The sphalerite microstructure indicates thermal overprinting, with no microbial structure being preserved. Thermal overprinting is also supported by stable isotope data and temperature calculations. Chemical zoning is related to fluctuating fluid composition or non-equilibrium rather than to a decreasing temperature trend.

6. Conclusions

For the Upper Permian of the NCA, the data indicate that the $\delta^{34}S$ isotopic composition of sulfates has a maxima of measured values between 11 and 12 ‰. The values for the gypsum-type and halite-type deposits are similar, indicating no major fractionation for the different salinity stages of the basin. Bacterial sulfate reduction is supported by the presence of sulfides and

https://doi.org/10.1017/S0016756816000996 Published online by Cambridge University Press

sulfur with low and variable $\delta^{34}S$ isotopic composition. Sulfates with $\delta^{34}S$ higher than 13 ‰ show remobilization features.

Lower Triassic, Röt-type sulfates are characterized by a heavy sulfur isotopic composition of *c*. 26 ‰. The present study supports the fact that these evaporites were widespread over the entire area of the NCA. Data compilation demonstrates that Röt-type evaporites formed in a large intracratonic stratified sea, with limited connectivity to the ocean.

The development of the sulfates of Carnian–Norian age from the CAM is more restricted in areal extent, and sulfates are characterized by $\delta^{34}S$ values of *c*. 15 ‰.

The mean value for $\delta^{18}O$ of sulfate from the halite-type deposit is 16.6 ‰, higher than in the gypsum-type deposits, with a mean of 14.5 ‰. Both delta values are higher than the oxygen isotopic composition of sulfates precipitated from present ocean water. $\delta^{18}O$ versus $\delta^{34}S$ trends support bacterial sulfate reduction and isotope exchange at relatively low temperatures. The oxygen isotope composition for the Lower Triassic Röt-type evaporites and for the Upper Triassic evaporites is similar between *c*. 15 ‰ and 16 ‰.

As a result of thermal overprinting and recrystallisation, bacterial structures are not preserved. However, isotopically, bacterial sulfate reduction was put in evidence. The sulfate–sulfide isotope thermometer indicates overprint temperatures of between 215 and 360 °C. Microbeam measurements show several generations of sphalerites related to fluctuating liquid chemistry rather than to variation in temperature.

Acknowledgements. CEEPUS mobility grant CIII-1415-80539 to UMCS Lublin is acknowledged. We appreciate constructive comments on the early version of the manuscript by Christophe Lecuyer and Tadeusz Peryt. Two anonymous reviewers are thanked for careful reading of the manuscript, and valuable comments and suggestions.

Supplementary material

To view supplementary material for this article, please visit https://doi.org/10.1017/S0016756816000996

References

Algeo, T. J., Luo, G. M., Song, H. S., Lyons, T. W. & Canfield, D. C. 2015. Reconstruction of secular variation in seawater sulfate concentrations. *Biogeosciences* **12**, 2131–51.

Ault, W. U. & Kulp, J. L. 1959. Isotopic geochemistry of sulphur. *Geochimica et Cosmochimica Acta* **16**, 201–35.

Bauer, F. K. 1967. Gipslagerstätten im zentralalpinen Mesozoikum (Semmering, Stanzertal). *Verhandlungen der Geologischen Bundesanstalt* **1967**, 70–90.

Berner, R. A. 1985. Sulfate reduction, organic matter decomposition and pyrite formation. *Philosophical Transactions of the Royal Society of London A* **315**, 25–38.

Boschetti, T. 2013. Oxygen isotope equilibrium in sulfate-water systems: a revision of geothermometric applications in low-enthalpy systems. *Journal of Geochemical Exploration* **124**, 92–100.

Boschetti, T., Cortecci, G., Toscani, L. & Iacumin, P. 2011. Sulfur and oxygen isotope compositions of Upper Triassic sulfates from northern Apennines (Italy): paleogeographic and hydrogeochemical implications. *Geologica Acta* **9**, 129–47.

Böttcher, M. E., Brumsack, H. J. & Dürselen, D. 2007. The isotopic composition of modern seawater sulfate: I. Coastal waters with special regard to the North Sea. *Journal of Marine Geology* **67**, 73–82.

Canfield, D. E. 2001. Biogeochemistry of sulphur isotopes. In *Stable Isotope Geochemistry* (eds J. W. Valley, D. R. Cole), pp. 579–606. Reviews in Mineralogy & Geochemistry 43.

Chiba, H. & Sakai, H. 1985. Oxygen isotope exchange rate between dissolved sulfate and water at hydrothermal temperatures. *Geochimica et Cosmochimica Acta* **49**, 993–1000.

Claypool, G. E., Holser, W. T., Kaplan, I. R., Sakai, H. & Zak, I. 1980. The age curves of sulfur and oxygen isotopes in marine sulfate and their mutual interpretation. *Chemical Geology* **28**, 199–260.

Cortecci, G., Reyes, E., Berti, G. & Casati, P. 1981. Sulfur and oxygen isotopes in Italian marine sulfates of Permian and Triassic ages. *Chemical Geology* **34**, 65–79.

Erkan, E. 1989. Die Sulfatlagerstätten der postvariszischen Transgressionsserie in den Ostalpen. *Nachrichten der Deutschen Geologischen Gesellschaft* **41**, 90–1.

Fanlo, I. & Ayora, C. 1998. The evolution of the Lorraine evaporite basin: implications for the chemical and isotope composition of the Triassic ocean. *Chemical Geology* **146**, 135–54.

Flügel, H. W. & Neubauer, F. 1984. *Steiermark Geologie der österreichischen Bundesländer in kurzgefassten Einzeldarstellungen*. Vienna: Geologische Bundesanstalt, 127 pp.

Fritz, P., Basharmal, G. M., Drimmie, R. J., Ibsen, J. & Qureshi, R. M. 1989. Oxygen isotope exchange between sulfate and water during bacterial reduction of sulfate. *Chemical Geology, Isotope Geoscience Section* **79**, 99–105.

García-Veigas, J., Cendón, D. I., Pueyo, J. J. & Peryt, T. M. 2011. Zechstein saline brines in Poland, evidence of overturned anoxic ocean during the Late Permian mass extinction event. *Chemical Geology* **290**, 189–201.

Gawlick, H.-J., Schlagintweit, F. & Suzuki, H. 2007. Die Ober-Jura bis Unter-Kreide Schichtfolge des Gebietes Höherstein-Sandling (Salzkammergut, Österreich) – implikationen zur rekonstruktion des Block-Puzzles der zentralen Nördlichen Kalkalpen, der Gliederung der karbonatischen Radiolaritflyschbecken und der Entwicklung der Plassen-Karbonatplattform. *Neues Jahrbuch für Geologie und Paläontologie Abhandlungen* **243**, 1–70.

Gawlick, H.-J., Lein, R., Piros, O. & Pytel, C. 1999. Zur stratigraphie und tektonik des Hallein – Bad Dürrnberger Salzberges – neuergebnisse auf der basis von stratigraphischen und faziellen daten (Nördliche Kalkalpen, Salzburg). *Abhandlungen der Geologischen Bundesanstalt* **56**(2), 69–90.

Gawlick, H.-J., Lein, R., Schlagintweit, F., Suzuki, H. & Wegerer, E. 2001. Der Hallstätter Salzberg und sein geologischer rahmen – geschichte und stand der erforschung, interpretationen und neue

ergebnisse. *Berichte der Geologischen Bundesanstalt* **56**, 45–9.

Gonfiantini, R. & Fontes, J., CH. 1963. Oxygen isotopic fractionation in the water of crystallisation of gypsum. *Nature* **200**, 644–6.

Götzinger, M. A. & Pak, E. 1983. Zur schwefelisotopenverteilung in sulfid- und sulfatmineralen triadischer Gesteine der Kalkalpen, Österreich. *Mitteilungen der Gesellschaft der Geologie- und Bergbaustudenten Österreichs* **29**, 191–8.

Grinenko, V. A. & Ustinov, V. I. 1991. Dynamics of sulfur and oxygen isotope fractionation during bacterial reduction. *Geochemistry International* **28**, 21–30.

Haditsch, J. G. 1968. Bemerkungen zu einigen mineralien (Devillin, Bleiglanz, Magnesit) aus der Gips-Anhydrit-Lagerstätte Wienern am Grundlsee. *Archiv für Lagerstättenforschung in den Ostalpen* **7**, 54–76.

Hagenguth, G. 1988. Die Gipsvorkommen bei Edelsdorf im Stanzertal (Steiermark). *Archiv für Lagerstättenforschung der Geologischen Bundesanstalt* **9**, 47–58.

Hałas, S. 1987. Oxygen and sulphur isotope ratios of sulphate minerals in native sulphur deposits. *Isotopenpraxis* **23**(7), 282–3.

Hałas, S. & Pluta, I. 2000. Empirical calibration of isotope thermometer $\delta^{18}O$ (SO_4^{2-}) – $\delta^{18}O(H_2O)$ for low temperature brines. In *ESIR Isotope Workshop V, 1–6 July 2000, Kraków, Poland, Book of Abstracts*, pp. 68–71.

Hałas, S. & Szaran, J. 2001. Improved thermal decomposition of sulfates to SO_2 and mass spectrometric determination of $\delta^{34}S$ of IAEA SO-5, IAEA SO-6 and NBS-127 sulfate standards. *Rapid Communications in Mass Spectrometry* **15**, 1618–20.

Hałas, S. & Szaran, J. 2004. Use of Cu_2O–$NaPO_3$ mixtures for SO_2 extraction from $BaSO_4$ for sulphur isotope analysis. *Isotopes in Environmental and Health Studies* **40**, 229–31.

Hałas, S., Szaran, J., Czarnacki, M. & Tanweer, A. 2007. Refinements in $BaSO_4$ to CO_2 preparation and $\delta^{18}O$ calibration of the sulphate standards NBS-127, IAEA SO-5 and IAEA SO-6. *Geostandard Geoanalytical Research* **31**, 61–8.

Hardie, L. A. 1996. Secular variation in seawater chemistry: an explanation for the coupled secular variation in the mineralogies of marine limestones and potash evaporites over the past 600 m.y. *Geology* **24**, 279–83.

Holland, H. D. 2005. Sea level, sediments and the composition of seawater. *American Journal of Science* **305**, 220–39.

Holser, W. T. 1977. Catastrophic chemical events in the history of the ocean. *Nature* **267**, 403–8.

Holser, W. T. & Kaplan, I. R. 1966. Isotope geochemistry of sedimentary sulfates. *Chemical Geology* **1**, 93–135.

Holser, W. T., Kaplan, I. R., Sakai, H. & Zak, I. 1979. Isotope geochemistry of oxygen in the sedimentary sulfate cycle. *Chemical Geology* **25**, 1–17.

Kajiwara, Y. & Krouse, H. R. 1971. Sulfur isotope partitioning in metallic sulfide systems. *Canadian Journal of Earth Sciences* **8**, 1397–408.

Kampschulte, A., Buhl, D. & Strauss, H. 1998. The sulfur and strontium isotopic compositions of Permian evaporites from the Zechstein basin, northern Germany. *Geologische Rundschau* **87**, 192–9.

Kampschulte, A. & Strauss, H. 2004. The sulfur isotopic evolution of Phanerozoic seawater based on the analysis of structurally substituted sulfate in carbonates. *Chemical Geology* **204**, 255–86.

Kirchner, E. 1987. Die mineral- und gesteinsvorkommen in den Gipslagerstätten der Lammermasse, innerhalb der Hallstattzone, Salzburg. *Jahrbuch Haus der Natur* **10**, 156–67.

Kirchner, E. C. 1979. Pumpellyitführende Kissenlavabreccien in der Gips-Anhydritlagerstätte von Wienern am Grundlsee, Steiermark. *Tschermaks Mineralogische und Petrographische Mitteilungen* **26**, 149–62.

Klaus, W. 1965. Zur einstufung alpiner salztone mittels sporen. *Verhandlungen der Geologischen Bundesanstalt, Sonderheft G*, 228–92.

Klaus, W. & Pak, E. 1974. Neue beiträge zur datierung von evaporiten des Ober-Perm. *Carinthia II* **164**(84), 79–85.

Kölbl, J. & Gawlick, H.-J. 1999. Bericht über geologische aufnahmen sowie stratigraphische und fazielle untersuchungen im bereich der meßnerin auf den blättern 101 eisenerz und 102 Aflenz kurort. *Jahrbuch der Geologischen Bundesanstalt* **142**, 346–8.

Kovalevych, V., Peryt, T. M., Beer, W., Geluk, M. & Hałas, S. 2002. Geochemistry of Early Triassic seawater as indicated by study of the Röt halite in the Netherlands, Germany, and Poland. *Chemical Geology* **182**, 549–63.

Kovalevich, V. M., Peryt, T. M. & Petrichenko, O. I. 1998. Secular variation in seawater chemistry during the Phanerozoic as indicated by brine inclusions in halite. *Journal of Geology* **106**, 695–712.

Kucha, H., Schroll, E., Raith, J. G. & Hałas, S. 2010. Microbial sphalerite formation in carbonate-hosted Zn–Pb ores, Bleiberg, Austria: micro- to nanotextural and sulfur isotope evidence. *Economic Geology* **105**, 1005–23.

Leitner, C. & Neubauer, F. 2011. Tectonic significance of structures within the salt deposits Altaussee and Berchtesgaden–Bad Dürrnberg, Northern Calcareous Alps. *Austrian Journal of Earth Sciences* **104**(2), 2–21.

Leitner, C., Neubauer, F., Genser, J., Borojevic-Sostaric, B. & Rantitsch, G. 2013. $^{40}Ar/^{39}Ar$ ages of recrystallization of rock-forming polyhalite in Alpine rocksalt deposits. In *Advances in 40Ar/39Ar Dating: From Archaeology to Planetary Sciences* (eds F. Jordan, D. F. Mark & C. Verati), pp. 207–44. Geological Society of London, Special Publication no. 378.

Lloyd, R. M. 1968. Oxygen isotope behaviour in the sulfate-water system. *Journal of Geophysical Research* **73**, 6099–110.

Longinelli, A. 1983. Oxygen-18 and sulphur-34 in dissolved oceanic sulphate and phosphate. In *The Marine Environment* (eds P. Fritz & J. C. Fonts), pp. 219–55. Handbook of Environmental Isotope Geochemistry. Amsterdam: Elsevier.

Longinelli, A. & Craig, H. 1967. Oxygen-18 variation in sulphate ions in sea water and saline lakes. *Science* **146**, 56–9.

Longinelli, A. & Flora, O. 2007. Isotopic composition of gypsum samples of Permian and Triassic age from the north-eastern Italian Alps: palaeoenvironmental implications. *Chemical Geology* **245**, 275–84.

Lowenstein, T. K., Hardie, L. A., Timofeeff, M. N. & Demicco, R. V. 2003. Secular variation in seawater chemistry and the origin of calcium chloride basinal brines. *Geology* **31**, 857–60.

Lowenstein, T. K., Kendal, B. & Anbar, A. D. 2014. The geologic history of seawater. In *The Oceans and Marine Geochemistry, 2nd Edition* (eds H. D. Holland & K. K. Turekian), pp. 569–622. Treatise on Geochemistry, Vol. 8. Amsterdam: Elsevier.

Machel, H. G., Krouse, H. R. & Sassen, R. 1995. Products and distinguishing criteria of bacterial and

https://doi.org/10.1017/S0016756816000996 Published online by Cambridge University Press

thermochemical sulphate reduction. *Applied Geochemistry* **110**, 373–9.

McCrea, J. M. 1950. On the isotopic geochemistry of carbonates and a paleotemperature scale. *Journal of Chemical Physics* **18**, 849–57.

Mizutani, Y. 1971. An improvement in the carbon reduction method for the isotopic analysis of sulfates. *Geochemical Journal* **5**, 69–7.

Niedermayr, G., Beran, A. & Brandstätter, F. 1989. Diagenetic type magnesites in the Permo-Scythian rocks of the Eastern Alps, Austria. In *Magnesite Geology, Mineralogy, Geochemistry, Formation of Mg-Carbonates* (ed. P. Möller), pp. 35–59. Monograph Series on Mineral Deposits. Berlin, Stuttgart: Gebrüder Bornträger.

Nielsen, H. 1965. Schwefelisotope im marinen Kreislauf und das $\delta^{34}S$ der früheren Meere. *Geologische Rundschau* **55**, 160–72.

Nielsen, H. 1989. Local and global aspects of the sulphur isotope age curve of oceanic sulphate. In *Evolution of the Global Biogeochemical Sulphur Cycle* (eds P. Brimblecombe, A. Yu Lein), pp. 57–64. SCOPE 39. New York: John Wiley & Sons Ltd.

Ohmoto, H. 1986. Stable isotope geochemistry of ore deposits. In *Stable Isotopes in High Temperature Geological Processes* (eds J. W. Valley, H. P. Taylor, Jr. & J. R. O'Neil), pp. 491–560. Reviews in Mineralogy 16.

Ohmoto, H. & Rye, R. O. 1979. Isotopes of sulfur and carbon. In *Geochemistry of Hydrothermal Ore Deposits* (ed. H. L. Barnes), pp. 517–612. New York: John Wiley & Sons Ltd.

Pak, E. 1974. Schwefelisotopenuntersuchungen am Institut für Radiumforschung und Kernphysik I. *Anzeiger der Akademie der Wissenschaften Mathematisch-Naturwissenschaftliche Klasse*, 166–174.

Pak, E. 1978. Schwefelisotopenuntersuchungen am Institut für Radiumforschung und Kernphysik II. *Anzeiger der Akademie der Wissenschaften Mathematisch-Naturwissenschaftliche Klasse*, 6–22.

Pak, E. 1981. Schwefelisotopenuntersuchungen am Institut für Radiumforschung und Kernphysik III. *Anzeiger der Akademie der Wissenschaften Mathematisch-Naturwissenschaftliche Klasse*, 187–98.

Pak, E. & Schauberger, O. 1981. Die geologische Datierung der ostalpinen Salzlagerstätten mittels Schwefelisotopenuntersuchungen. *Verhandlungen der Geologischen Bundesanstalt* **1981**, 185–92.

Payne, J. L., Lehrmann, D. J., Wei, J., Orchard, M. J., Schrag, D. P. & Knoll, A. H. 2004. Large perturbations of the carbon cycle during recovery from the end-Permian extinction. *Science* **305**, 506–9.

Paytan, A., Kastner, M., Campell, D. & Thiemens, M. H. 2004. Seawater sulfur isotope fluctuations in the Cretaceous. *Science* **304**, 1663–5.

Peryt, T. M., Hałas, S. & Hryniv, S. P. 2010. Sulphur and oxygen isotope signatures of late Permian Zechstein anhydrites, West Poland: seawater evolution and diagenetic constraints. *Geological Quarterly* **54**, 387–400.

Postl, W. 1990. Enargit und Parnauit aus dem Gips- und Anhydritbergbau Tragöß-Oberort, Steiermark. In *Neue Mineralfunde aus Österreich XXXIX* (eds G. Niedermayr, F. Brandstätter, G. Kandutsch, E. Kirchner, B. Moser & W. Postl), p. 277. *Carinthia II* **180**(100), 245–88.

Prokoph, A., Shields, G. A. & Veizer, J. 2008. Compilation and time series analysis of a marine carbonate $\delta^{18}O$, $\delta^{13}C$, $^{87}Sr/^{86}Sr$ and $\delta^{34}S$ database through Earth history. *Earth-Science Reviews* **87**, 113–33.

Pueyo, E. L., Mauritsch, H. J., Gawlick, H.-J., Scholger, R. & Frisch, W. 2007. New evidence for block and thrust sheet rotations in the central northern Calcareous Alps deduced from two pervasive remagnetization events. *Tectonics* **26**, doi: 10.1029/2006TC001965.

Raab, M. & Spiro, B. 1991. Sulfur isotopic variations during seawater evaporation with fractional crystallization. *Chemical Geology* **86**, 323–33.

Rafter, T. A. & Mizutani, Y. 1967. Preliminary study of variations of oxygen and sulphur isotopes in natural sulphates. *Nature* **216**, 1000–2.

Rees, C. E., Junkins, W. J. & Monster, J. 1978. The sulphur isotopic composition of ocean water sulphate. *Geochimimica et Cosmochimica Acta* **42**, 377–82.

Rey, K., Amiot, R., Fourel, F., Rigaudier, T., Abdala, F., Day, M. O., Fernandez, V., Fluteau, F., France-Lanord, C., Rubidge, B. S., Smith, R. M., Viglietti, P. A., Zipfel, B. & Lécuyer, C. 2016. Global climate perturbations during the Permo-Triassic mass extinctions recorded by continental tetrapods from South Africa. *Gondwana Research* **37**, 384–96.

Sakai, H. 1968. Isotopic proprieties of sulfur compounds in hydrothermal processes. *Geochemical Journal* **2**, 29–49.

Schauberger, O. 1986. Bau und Bildung der Salzlagerstätten des ostalpinen Salinars. *Archiv für Lagerstättenforschung der Geologischen Bundesanstalt* **7**, 217–54.

Schorn, A. & Neubauer, F. 2011. Emplacement of an evaporitic melange nappe in central Northern Calcareous Alps: evidence from the Moosegg klippe (Austria). *Journal of Austrian Earth Sciences* **104**, 22–46.

Schorn, A., Neubauer, F., Bernroider, M. & Genser, J. 2012. The sulphatic Haselgebirge evaporite mélange of the Moosegg quarry, central Northern Calcareous Alps. *Field Guide, Pangeo*, 20 pp.

Scholle, P. A. 1995. Carbon and sulfur isotope stratigraphy of the Permian and adjacent intervals. In *The Permian of Northern Pangea*, Vol. 1 (eds P. A. Scholle, T. M. Peryt & D. S. Ulmer Scholle), pp. 133–149. Berlin: Springer.

Schorn, A., Neubauer, F., Genser, J. & Bernroider, M. 2013. The Haselgebirge evaporitic mélange in central Northern Calcareous Alps (Austria): part of the Permian to Lower Triassic rift of the Meliata ocean? *Tectonophysics* **583**, 28–48.

Seal, R. R., Alpers, C. N. & Rye, R. O. 2000. Stable isotope systematics of sulfate minerals. In *Sulphate Minerals: Crystallography, Geochemistry, and Environmental Significance* (eds C. N. Alpers, J. L. Jambor & D. K. Nordstrom), pp. 541–93. Reviews in Mineralogy and Geochemistry 40.

Sharp, Z. D. 2014. Stable isotope techniques for gas source mass spectrometry. In *Analytical Geochemistry/Inorganic INSTR. Analysis* (eds H. D. Holland & K. K. Turekian), pp. 291–307. Treatise on Geochemistry, 2nd Edition, Vol. 15. Amsterdam: Elsevier.

Song, H., Wignall, P. B., Tong, J., Bond, D. P. G., Song, H., Lai, X., Zhang, K., Wang, H. & Chen, Y. 2012. Geochemical evidence from bio-apatite for multiple oceanic anoxic events during Permian–Triassic transition and the link with end-Permian extinction and recovery. *Earth and Planetary Science Letters* **353**, 12–21.

Spötl, C. 1988*a*. Zur Altersstellung permoskythischer Gipse im Raum des östlichen Karwendelgebirges (Tirol). *Geologisch Paläontologische Mitteilungen Innsbruck* **14**(9), 197–212.

Spötl, C. 1988*b*. Schwefelisotopendatierung und fazielle Entwicklung permoskythischer Anhydrite in den Salzbergbauen von Dürnberg (Hallein) und Hallstatt (Österreich). *Mitteilungen der Gesellschaft der Geologie- und Bergbaustudenten Österreichs* **34**(35), 209–29.

Spötl, C. 1988*c*. Evaporitische Fazies der Reichenhaller Formation (Skyth/Anis) im Haller Salzberg (Nördliche Kalkalpen, Tirol). *Jahrbuch der Geologischen Bundesanstalt* **131**, 153–68.

Spötl, C. 1989*a*. The Alpine Haselgebirge Formation, Northern Calcareous Alps (Austria): Permo-Scythian evaporites in an alpine thrust system. *Sedimentary Geology* **65**, 113–25.

Spötl, C. 1989*b*. Die Salzlagerstätte von Hall in Tirol – ein Überblick über den stand der geologischen erforschung des 700 jährigen Bergbaubetriebes. *Veröffentlichungen des Tiroler Landesmuseums Ferdinandeum* **69**, 137–67.

Spötl, C. & Pak, E. 1996. A strontium and sulfur isotopic study of Permo-Triassic evaporites in the Northern Calcareous Alps. *Chemical Geology* **131**, 219–34.

Strauss, H. 1997. The isotopic composition of sedimentary sulfur through time. *Palaeogeography, Palaeoclimatology, Palaeoecology* **132**, 97–118.

Syverson, D. D., Ono, S., Shanks, W. C. & Seyfried, W. E. 2015. Multiple sulfur isotope fractionation and mass transfer processes during pyrite precipitation and recrystallization: an experimental study at 300 and 350 °C. *Geochimica et Cosmochimica Acta* **165**, 418–34.

Szaran, J., Niezgoda, H. & Hałas, S. 1998. New determination of oxygen and sulphur isotope fractionation between gypsum and dissolved sulphate. *ESIR Isotope Workshop IV, Portorož, June 1998, RMZ Materials and Geoenvironment* **45**, 180–2.

Thode, H. G. & Monster, J. 1965. Sulphur-isotope geochemistry of petroleum, evaporites, and ancient seas. *American Association of Petroleum Geologists Memoirs* **4**, 367–77.

Tollmann, A. 1977. *Geologie von Österreich. Band 1. Die Zentralalpen*. Wien: Deuticke, 766 pp.

Weber, L. (ed.) 1997. Handbuch der Lagerstätten, der Erze, Industrieminerale und Energierohstoffe Österreichs. *Archiv für Lagerstättenforschung der Geologischen Bundesanstalt* **19**, 607 pp.

Zeebe, R. E. 2010. A new value for the stable oxygen isotope fractionation between dissolved sulfate ion and water. *Geochimica et Cosmochimica Acta* **74**, 818–28.

https://doi.org/10.1017/S0016756816000996 Published online by Cambridge University Press